Powder Technology 395 (2022) 338–347

Contents lists available at ScienceDirect

Powder Technology

journal homepage: www.elsevier.com/locate/powtec

Preparation of the rod-shaped SiO_2@C abrasive and effects of its microstructure on the polishing of zirconia ceramics

Lei Xu [a,b,c], Hong Lei [a,b,*], Zhengyu Ding [b], Yi Chen [b], Ruyue Ding [b], Taesung Kim [c,d]

[a] School of Materials Science and Engineering, Shanghai University, Shanghai 200444, China
[b] Research Center of Nano Science and Technology, Shanghai University, Shanghai 200444, China
[c] School of Mechanical Engineering, Sungkyunkwan University, Gyeonggi-do 16419, Republic of Korea
[d] SKKU Advanced Institute of Nanotechnology, Sungkyunkwan University, Gyeonggi-do 16419, Republic of Korea

ARTICLE INFO

Article history:
Received 14 July 2021
Received in revised form 14 September 2021
Accepted 29 September 2021
Available online 30 September 2021

Keywords:
Rod-shaped abrasive
Carbon-coated silica
Polishing
Zirconia ceramic
Line contact
Elastic contact

ABSTRACT

This study aims to achieve higher-efficiency zirconia ceramic polishing demands, using a novel rod-shaped SiO_2@C abrasive that was synthesized by a simple three-step method. The scanning electron microscopy and transmission electron microscopy results showed that composite abrasives were rod-shaped. As confirmed by Fourier transform infrared spectrometer and Raman spectra, the composite particle had a core-shell structure with a core of silica and a shell of carbon. According to the N_2 adsorption-desorption results, this composite abrasive had a mesoporous structure. The material removal rate of 242.5 nm/h and the zirconia ceramic surface roughness of 1.86 nm are 70.4% higher and 27.9% lower, respectively, than those achieved with conventional silica abrasives. The improved polishing performance may be attributed to its line contact mode, the reduction of Young's modulus and the improvement of tribochemical reaction. This study highlights the interaction between the surface microstructure of abrasives and the surface planarization of ceramics.

1. Introduction

Zirconia ceramics are considered to be one of the main candidate materials for back ceramic covers of 5G mobile phones, and they are highly regarded for their advantages of lightness, hardness, wear resistance, low signal shielding effect, great heat dissipation, and good texture [1]. Pure zirconia materials undergo a crystal transformation during heating and cooling, causing volume changes, which easily cracks the ceramic [2]. Therefore, doping is often used to inhibit phase transition and improve the toughness of zirconia ceramics [3–5]. Mobile phone back covers usually require a smoother surface and mirror effect. However, it is difficult for modified zirconia ceramics to meet such requirements due to their high mechanical strength and fracture toughness requirements. Therefore, ultra-precision grinding and lapping were usually carried out in the initial stage to make the crystals or ceramics have a satisfactory surface shape [6–8]. Then the polishing technology was used to obtain a better surface quality. Chemical mechanical polishing (CMP) is considered to be an effective method to achieve atomic-level smooth surfaces on hard and brittle materials [9]. It is an ultra-precision processing technology that can combine mechanical and chemical action to achieve global planarization. CMP is widely used in optical instruments [10–12], integrated circuits [13–16], electronic instruments [17], ceramics [18,19] and other fields.

In CMP technology, abrasives in the slurry are considered to be important factors affecting the polishing efficiency of the workpiece. Silica nanoparticles are one of the main abrasives used in CMP slurries. They have the advantages of good dispersibility, stability, moderate hardness, and low cost, and can achieve high-quality surfaces [12,20]. However, the material removal rates that can be achieved by conventional silica abrasives no longer meet the ever-increasing polishing rate demands. For this reason, Liang et al. synthesized non-spherical silica abrasives by a cation induction method and compared them with spherical abrasives. They showed that the material removal rate (MRR) of non-spherical abrasives increased by 65% [21]. Salleh et al. compared spherical and non-spherical silica abrasives when polishing hard disks. They found that non-spherical silica abrasives had a higher friction coefficient, and the MRR increased by 20% compared with spherical abrasives [22]. In our past work, there have also been synthesized silica with various morphologies: flower-shaped [23], popcorn-like [24] and these single particles are non-spherical particles. Both are controlled by the introduction of non-ionic surfactants. Although the MRR increased at that time, it still had a certain inhibitory effect because the non-ionic surfactant would adsorb on the surface of the workpiece to form a passivation layer [24,25]. After trying these previous abrasives, it was also

* Corresponding author at: School of Materials Science and Engineering, Shanghai University, Shanghai 200444, China.
E-mail address: hong_lei2005@aliyun.com (H. Lei).

https://doi.org/10.1016/j.powtec.2021.09.070
0032-5910/

found that the removal ability of non-spherical abrasives was indeed weakened. Although the above-mentioned non-spherical abrasives increased the MRR, the surface flatness of the workpiece has not been improved much and even slightly decreased in some cases.

In recent years, the core-shell structure of non-rigid composite abrasives has become a research hotspot for many scientists seeking to improve the surface quality of the workpiece. The elastic modulus, Poisson's ratio, hardness and other properties suggest that the special structure of the organic/inorganic core-shell composite abrasives result in elastic contact between the abrasives and the polished workpiece [26–28]. In turn, a damage-free surface of the workpiece can be realized, and the average surface roughness (Ra) can be greatly reduced. However, such non-rigid mechanical properties often lead to poor polishing rates. Therefore, simultaneously improving the surface quality and polishing rate is the focus of research into CMP applications.

In this article, the non-spherical and core-shell structures are combined for the first time to modify the silica abrasives in multiple steps. Based on the microemulsion template method [23], rod-shaped silica seeds are prepared and then textured with active silicic acid [29]. Numerous rough spots are formed on the rod, which are calcined on rod-shaped silica abrasives under air to form a carbon shell. The effect of different C coating amounts on the ceramic CMP was explored, and the polishing mechanism of rod-shaped SiO_2@C abrasives (RSSC) was analyzed based on the morphology and structure of the abrasive.

2. Experimental section

2.1. Materials

We used the following experimental materials: polyvinyl pyrrolidone (PVP, $(C_6H_9NO)_n$, 30 K, Sinopharm Chemical Reagent Co., Ltd., China), n-pentanol ($C_5H_{11}OH$, analytical reagent, Sinopharm Chemical Reagent Co., Ltd.), absolute ethanol (C_2H_5OH, analytical reagent, Sinopharm Chemical Reagent Co., Ltd.), deionized water (DI), sodium citrate ($Na_3C_6H_5O_7 \cdot 2H_2O$, Sinopharm Chemical Reagent Co., Ltd.), an aqueous ammonia solution (30%, Sinopharm Chemical Reagent Co., Ltd.), tetraethyl orthosilicate (TEOS, $C_8H_{20}O_4Si$, analytical reagent, Sinopharm Chemical Reagent Co., Ltd.), a cation exchange resin (Sinopharm Chemical Reagent Co., Ltd.), sodium silicate (Na_2SiO_3, JiNan DeWang Chemical Industry Co., Ltd., China), sodium hydroxide (NaOH, Sinopharm Chemical Reagent Co., Ltd.), and hydrochloric acid (HCl, analytical reagent, Sinopharm Chemical Reagent Co., Ltd.).

2.2. Preparation of rod-shaped SiO_2@C abrasives

The preparation process was carried out in multiple steps. First, rod-shaped silicon oxide seeds were prepared by the water-in-oil (W/O) microemulsion method. A typical synthesis was conducted as follows. Specifically, 15 g PVP was added to a three-necked flask containing 150 ml n-pentanol and was dissolved by ultrasound. After the PVP had completely dissolved, 15 ml ethanol, 4.2 ml deionized water, 1.5 ml 0.18 mol/l sodium citrate solution and 3 ml ammonia were added in sequence. Each time a reagent was added, the solution was stirred for 5 min. Finally, 2 ml TEOS was added and stirred at high speed, and the reaction was left standing at room temperature for 24 h to obtain the initial rod-shaped silica seeds.

In the second step, an oil-in-water (O/W) microemulsion method was used to prepare rod-shaped silica textured with silicic acid. In addition, 2.5 wt% active silicic acid was prepared in advance through a cation exchange resin. The rod-shaped silica seeds obtained in the first step were placed in a four-mouth flask, and 1000 ml deionized water was added, stirred and heated to boil. Then, 1600 ml 2.5 wt% silicic acid was dropped into it at a constant speed of 6.7 ml/min by a constant pressure funnel, consistent with the water evaporation speed. At the same time, a 3 wt% NaOH solution was added drop-wise to maintain the pH at about 10, and finally a textured rod-shaped silica sol was obtained.

In the last step, the textured rod-shaped silica sol was freeze-dried and then calcined in a muffle furnace at 500 °C for 2 h to obtain a carbon-coated rod-shaped silica powder. Finally, the powder was added to deionized water for ball grinding, and it was prepared into a rod-shaped SiO_2@C slurry with a solid content of 5 wt%, which was used for polishing experiments.

In this experiment, a certain amount of PVP was added again before freeze-drying to explore the influence of different carbon coating contents on the polishing performance of abrasives, and a series of rod-shaped SiO_2@C abrasives with different carbon coating contents were prepared.

2.3. Polishing tests

All polishing experiments were performed on a UNIPOL-1000S CMP polishing machine provided by Shenyang Kejing Instrument Co., Ltd., China. For comparison, a conventional spherical silica sol provided by ZheJiang DeLiXin Micro/Nano Science and Technology Co., Ltd., China and a series of rod-shaped SiO_2@C slurries (the solid contents were all 5 wt%) were selected, and the pH values of the slurries were adjusted to 10 with a 3 wt% NaOH solution. In this experiment, the polishing pad was a Rodel porous polyurethane pad. The polishing parameters were set as follows: the load pressure was 6 kg, the upturn speed was 30 rpm, the downturn speed was 60 rpm, the polishing time was 2 h, and the feed rate of the slurry was 180 ml/min. After the experiments, the zirconia ceramics were ultrasonically cleaned in ethanol for 30 min. Finally, they were dried and cooled to room temperature.

2.4. Characterization

The morphologies of rod-shaped silica seed crystals, textured rod-shaped silica, and RSSC were characterized by scanning electron microscopy (Nova NanoSEM 450, FEI, USA) at an acceleration voltage of 10 kV. The surface morphologies and core-shell structures of RSSC were further observed at an acceleration voltage of 200 kV by transmission electron microscopy (TEM, JEM-2100F, Japan). Thermogravimetric analysis of RSSC was carried out on a synchronous thermal analyzer (DSC/DTA-TG STA449F5, Netzsch, Germany) in an air atmosphere at a heating rate of 10 °C/min from 20 °C to 800 °C. Nitrogen adsorption-desorption isotherms of the samples were measured at −196 °C using an automatic surface and pore size analyzer (Autosorb-IQ2, Quantachrome Corporation), and the specific surface area of the samples was calculated by the Brunauer-Emmett-Teller (BET) method. The RSSC was qualitatively analyzed in the range of 4000 to 400 cm^{-1} using a Fourier transform infrared spectrometer (FTIR Avatar 370, Nicolet, USA). The carbon shell was characterized by laser confocal Raman spectroscopy (Senterra R200-L, Bruker Optics, Germany) using a He-Ne laser with a wavelength of 632.8 nm at a relative power of 50% for a duration 25 s. All the samples for characterization were cleaned by centrifugation three times with deionized water and were finally dried for testing. The surface morphologies of the polished and unpolished zirconia ceramics were measured using a metallographic microscope (CMM-50, Shanghai Changfang Optical instrument Co., Ltd., China) and an Ambios Xi-100 surface profiler (Ambios Technology Corp., USA) with a resolution of 0.1 Å, a focal depth of 3.0 μm, and a working distance of 4.9 mm over a measurement area of 100 μm × 100 μm. In our previous work [30], we introduced a self-made instrument that can approximately measure the coefficient of friction between zirconia ceramics, abrasives and the polishing pad. For preparing samples for the measurements, the same amount of each slurry sample was dropped on the surface of the zirconia ceramic and dried at 60 °C. The force curve was recorded by an atomic force microscope (NX10; Park Systems Corp., Korea) under a force of 500 nN at a speed of 0.2 μm/s. We selected 20 effective force curves and used AFM analysis software to fit and calculate the

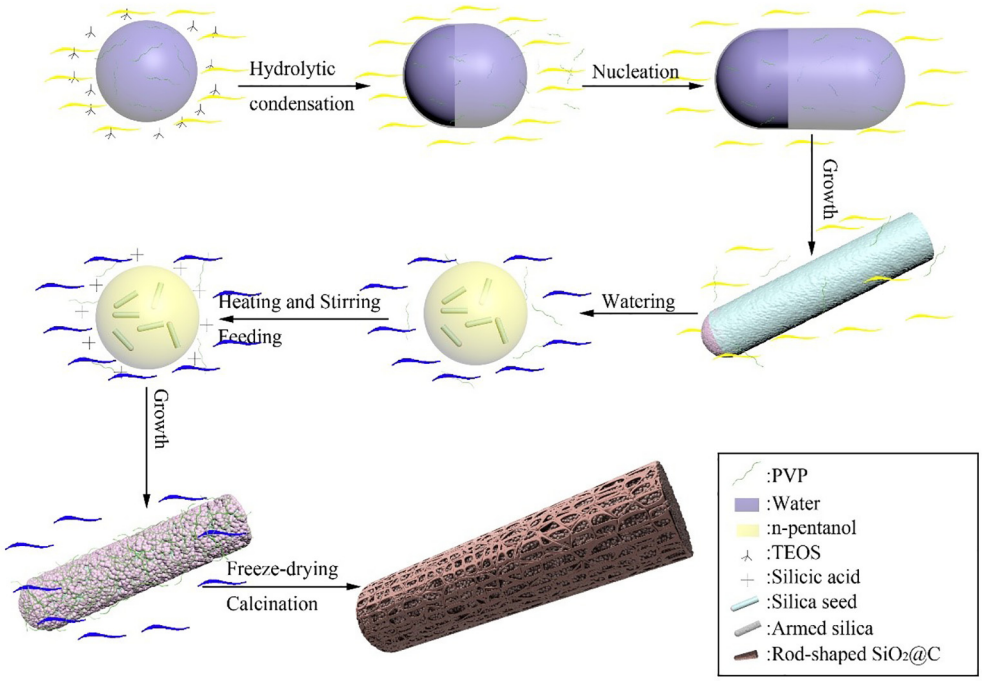

Scheme 1. Flow chart demonstrating preparation of rod-shaped carbon-coated silica abrasives.

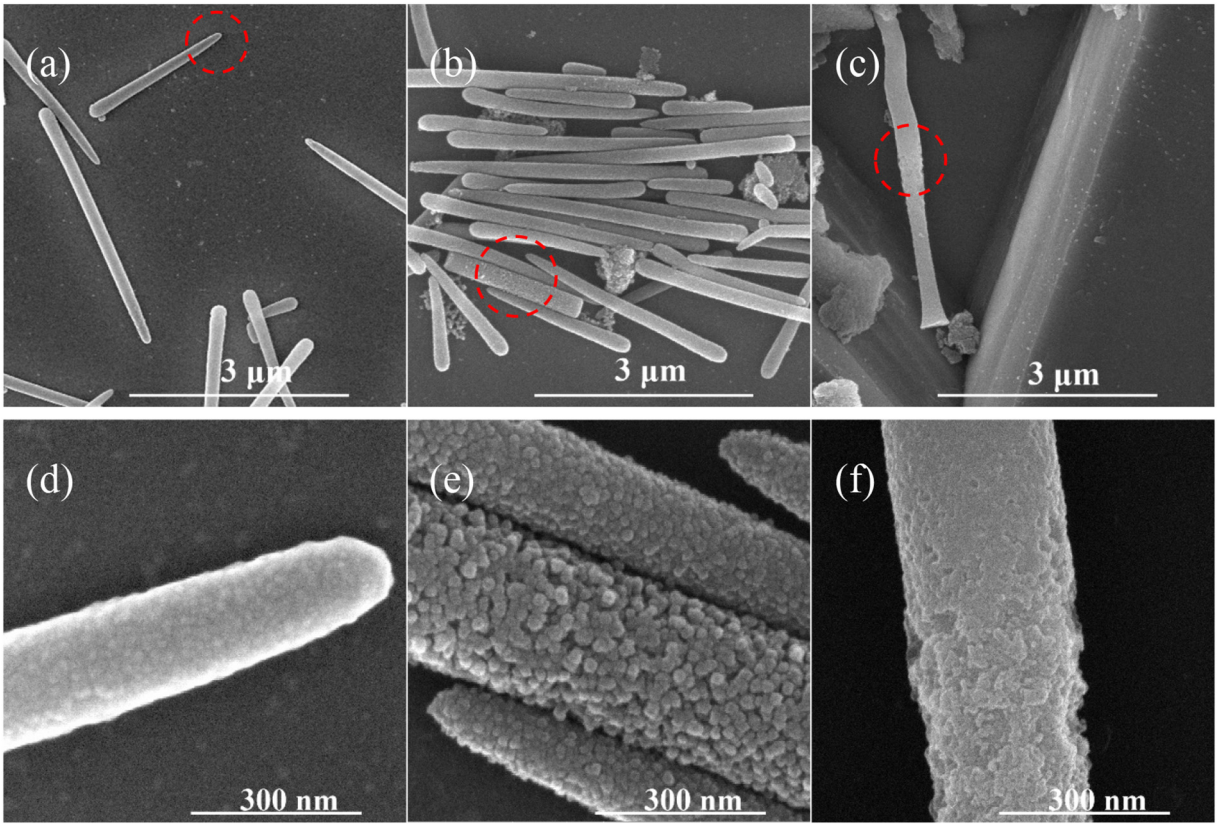

Fig. 1. SEM micrographs of silica particles at various stages. (a) Silica seeds in the first step. (b) Silica particle texturing in the second step. (c) RSSC abrasives used in the polishing experiment. (d–f) Enlarged SEM images of particles corresponding to the three steps shown in (a), (b) and (c), respectively. (The dotted red circles represent the positions of (d), (e) and (f) intercepted in (a), (b) and (c), respectively.)

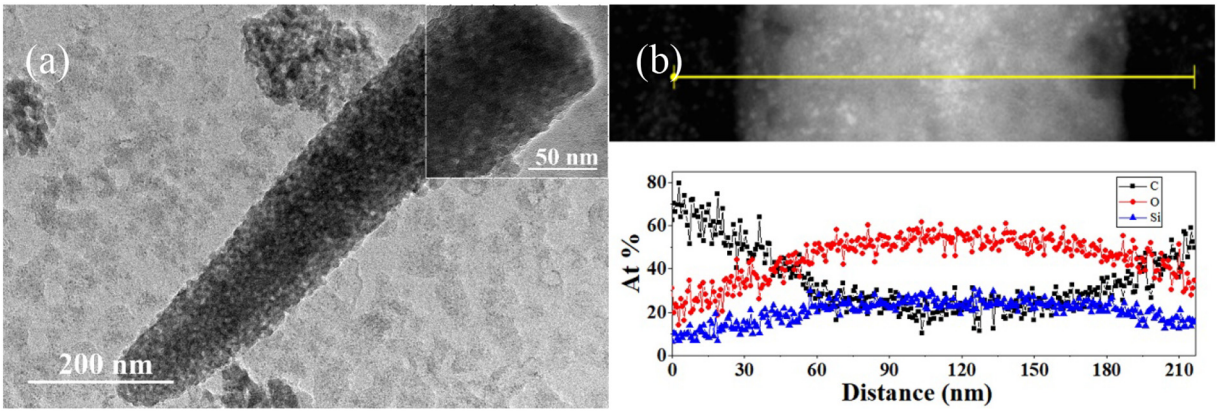

Fig. 2. (a) TEM image and enlarged TEM image (inset) of the RSSC abrasive. (b) EDS spectrum image of the RSSC abrasive.

corresponding Young's modulus (E) to obtain the average value. Since the exact Poisson's ratio (ν) of the RSSC abrasives was unknown, the ν value of the silica material (0.15) was used in the fitting for calculation. Subsequently, the water contact angle test was performed on the abrasives dried on the zirconia ceramics. Water contact angles of all samples were measured using a goniometer (Attension Theta Flex, Sweden). Each sample was measured 3 times to calculate the average value.

3. Results and discussion

3.1. Synthesis mechanism of RSSC

The double-system microemulsion template method was applied in a previous study [23]. In this article, we used this method to synthesize rod-shaped silica particles, and then the final rod-shaped carbon coated silica abrasives were prepared by freeze-drying and calcination. A flowchart illustrates the steps of the procedure for preparation of RSSC abrasives in Scheme 1. The first step in the synthesis of rod silica seeds in the W/O system has been well studied [31,32]. Initially, small water droplets stabilized by sodium citrate and PVP in n-pentanol exist synergistically in n-pentanol; then, PVP moves from n-pentanol to the water phase. The TEOS added later is soluble in n-pentanol and is then hydrolyzed to form nuclei on the surface of the water-rich emulsion droplets. Since TEOS in hydrolyzed form only exists in the water phase at the other end of the emulsion, it provides the silica a nucleus for unilateral growth and finally forms rod-shaped silica seeds. The second step is to further grow rod-shaped silica seeds in the O/W system. The rod-shaped silica seed obtained in the first step first forms small oil droplets in water, and then the silicic acid added drop-wise is preferentially dissolved in water for further reaction. Based on Ostwald ripening theory, the smaller particles in the sol are dissolved and re-deposited on the larger sol particles [33,34]. Silicic acid will further grow on rod-shaped silica seeds. Because of the instability of the oil-water interface, the silicic acid condensation reaction is asymmetric, and the rod-shaped silica will eventually form an uneven surface. In the third step, a carbon-coated structure is formed by freeze-drying and calcination. After the reaction, a large amount of PVP still exists in the obtained solution. Because the pyrrolidone in the PVP molecular chain unit contains lactam, it can form a strong hydrogen bond with the hydroxyl group on the surface of the silica, and PVP will attach to the rod-shaped silica. Furthermore, freeze-drying can leave PVP on the surface of the silica, forming a carbon shell covering the silica core in the final calcination [34]. Below we describe the qualitative analysis of RSSC, various characterizations, and we verify the synthesis principles.

3.2. Silica morphology

Fig. 1 shows SEM micrographs of silica particles at various stages. Fig. 1(a) shows the silica seeds obtained in the first step. These have a rod-shaped morphology with diameters of 150–200 nm and lengths of 3 μm, in line with the results reported in the literature. Fig. 1(b) shows the morphology of silica particles reacted with silicic acid obtained in the second step. The particles are also rod-shaped, with no obvious changes in diameter and size. Fig. 1(c) shows the morphologies of carbon-coated rod-shaped silica abrasives used in the polishing experiment. The shapes and sizes of the particles did not change significantly compared to the previous two particles. Fig. 1(d) and (e) are enlarged SEM images of silica seeds and textured silica particles, respectively. After the growth of silicic acid, the surface of the smoother silica seed is densely packed with extremely small particles and becomes rough and uneven, and the term 'textured' is used to describe this. The enlarged SEM image in Fig. 1(f) shows that the surface of the RSSC particles no longer clearly show the outline of the attached small particles, and the surface seems to be covered with a shell layer.

Fig. 2 shows a TEM image of rod-shaped SiO_2@C abrasives, and the observed morphology and size are consistent with the SEM images in Fig. 1. The dotted line in Fig. 2(a) represents the border of the enlarged TEM inset image. The particles have a core-shell structure with uniform

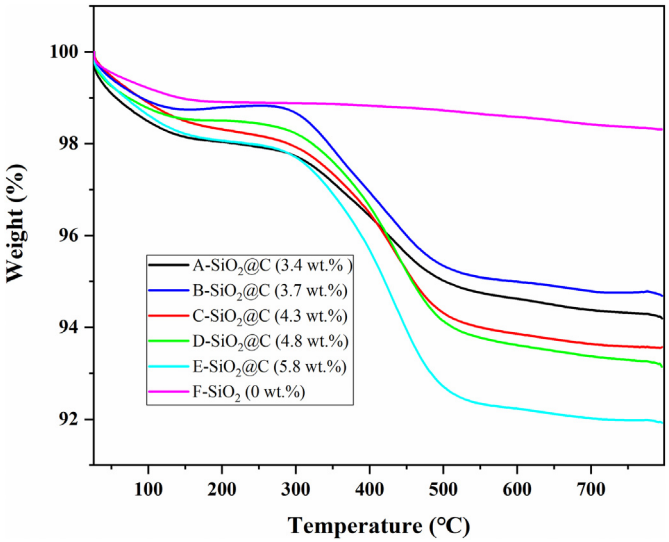

Fig. 3. TGA curves of SiO_2@C abrasives with different carbon contents.

Table 1
Detailed surface areas and pore diameters of samples.

Sample	Carbon coating content (wt%)	Surface area (m^2/g)	Pore diameters (nm)
A-SiO_2@C	3.4	102.57	13.18
B-SiO_2@C	3.7	104.80	10.01
C-SiO_2@C	4.3	117.65	10.06
D-SiO_2@C	4.8	150.12	8.99
E-SiO_2@C	5.8	151.63	10.10
F-SiO_2	0	102.02	13.15

pores. Combined with the EDS spectrum in Fig. 2(b), the atomic fraction distribution of C is low in the middle and high on both sides, while the atomic fraction distribution of Si and O is high in the middle and low on both sides; the Si to O ratio is 1:2. According to the EDS spectrum, the core of the RSSC abrasive is silica, and the shell is carbon. This shows that PVP is indeed adsorbed on the surface of textured silica particles and forms a carbon shell to coat the particles after calcination.

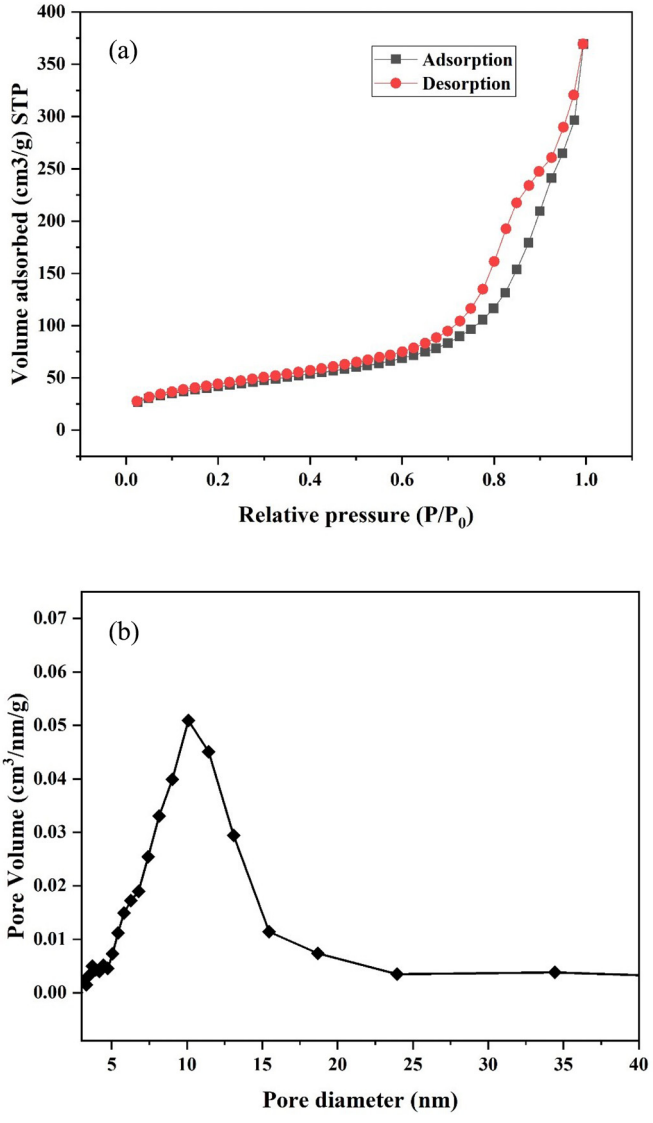

Fig. 4. (a) N_2 adsorption-desorption isotherms and (b) the corresponding pore size distribution of *E*-SiO_2@C abrasives.

3.3. TGA measurement

TGA curves were obtained to measure the carbon content of the shell on RSSC abrasives and explore the influence of different carbon contents on polishing. Fig. 3 shows TGA curves of the rod-shaped carbon coated silica abrasives calcined at different PVP contents. The A-E series (ordered by the amount of PVP from low to high) of SiO_2@C abrasives were particles calcined for 2 h, while F-SiO_2 was pure rod-shaped silica abrasives calcined for 12 h, and its carbon content was 0 wt%. As can be seen from Fig. 3 at 20–150 °C, the weight loss of all particles was approximately 1.5 wt%, which was caused by the loss of moisture from the air adsorbed on the surface and pores of particles. The A-E series samples began to lose weight in the second stage at 300 °C. Among them, the weight loss of *E*-SiO_2@C was the highest (5.8 wt%). These weight losses were caused by the thermal decomposition of the carbon layer on the silica surface in the air. Moreover, the order of the weight loss (A-SiO_2@C (3.4 wt%) < B-SiO_2@C (3.7 wt%) < C-SiO_2@C (4.3 wt%) < D-SiO_2@C (4.8 wt%) < E-SiO_2@C (5.8 wt%)) was consistent with the amount of PVP. These results provided further supporting evidence for the successful coating of the carbon shell on the surface of the silica core.

3.4. Surface area and pore size distribution

The specific surface areas of A-E series SiO_2@C particles and pure rod-shaped silica particles were further investigated by nitrogen adsorption-desorption measurements, and the pore size distribution was calculated by the Barrett-Joyner-Halenda (BJH) method. According to the IUPAC classification, all six samples display typical type-IV isotherms with H3-type hysteresis loops (Fig. S1), which indicate the existence of mesoporous structures in the particles. In addition, Fig. S2 shows that the pore size distribution of all particles is uniform. More detailed data are presented in Table 1. As the content of carbon coating increased, the specific surface area of the RSSC abrasives gradually increased, and the pore diameters were all around 10 nm.

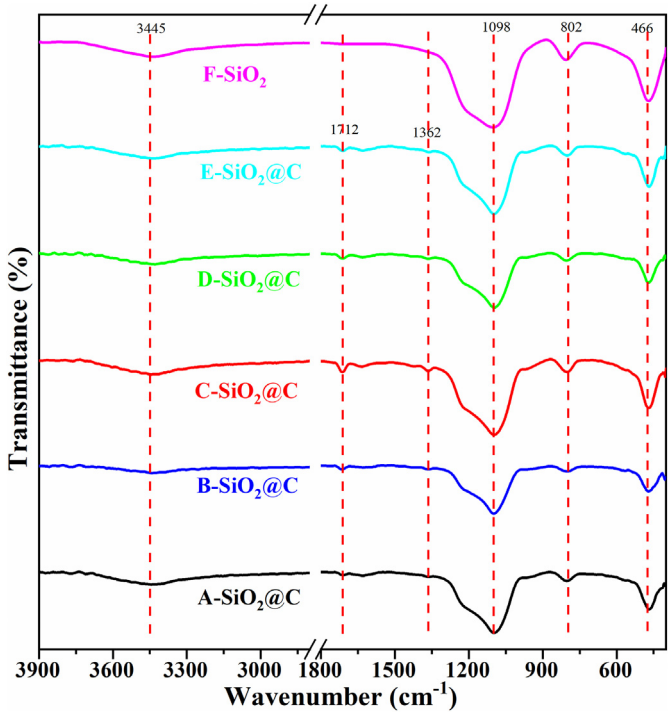

Fig. 5. FTIR spectra of all six samples.

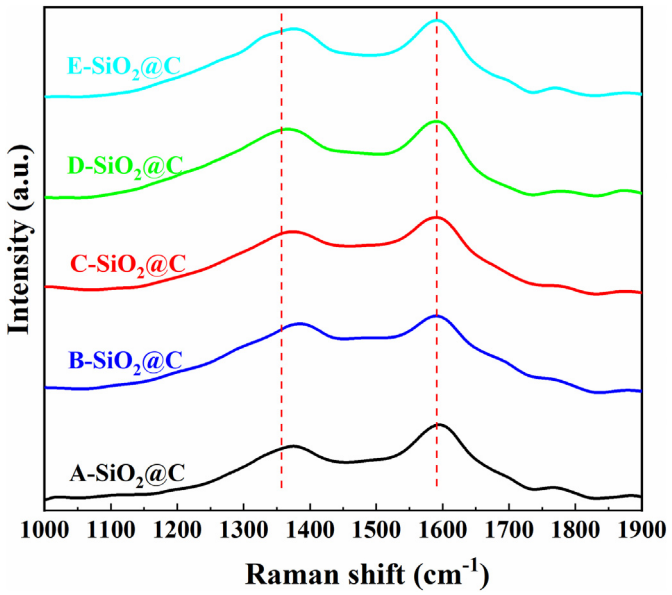

Fig. 6. Raman spectra of A-E series SiO_2@C particles.

Fig. 4(a) shows the type IV isotherm of *E*-SiO_2@C, which has the highest carbon shell content. A smooth capillary condensation step at $P/P_0 = 0.6–1.0$ can be observed, which corresponds to a broad pore size distribution at 10 nm in Fig. 4(b). The nitrogen adsorption/desorption measurements indicate that E-SiO_2@C particles possess a specific surface area of 151.63 m^2/g, which is much larger than that of pure rod-shaped silica abrasives. This is mainly due to the carbon shell covering the surface of the silica. PVP formed a porous carbon layer after calcination, which further increased the specific surface area of the particles. Based on BET and TEM analyses, we conclude that the RSSC abrasives show a well-structured nanoarchitecture with a very high specific surface area.

3.5. Spectroscopic characterization

The chemical compositions of A-E series SiO_2@C and F-SiO_2 particles were further characterized by FTIR analysis. The peak in Fig. 5 at 3445 cm^{-1} is attributed to the antisymmetric stretching vibration of Si-OH. The peaks at 1098 cm^{-1} and 802 cm^{-1} are attributed to the antisymmetric stretching vibration and the symmetric stretching vibration of Si-O-Si, respectively. The peak at 466 cm^{-1} is assigned to the flexural vibration of Si-O-Si, which verifies the presence of the silica structure. For all samples, the characteristic peaks of PVP (approximately 1420, 2880, and 2955 cm^{-1} in Fig. S3) disappear, indicating that the PVP has been completely carbonized by calcination. In addition, in the FTIR spectra of A-E series SiO_2@C particles, the peak at 1712 cm^{-1} is attributed to the stretching vibration of C═O, and the characteristic peak at 1362 cm^{-1} was assigned to aromatic C-N stretching vibration. These are characteristic peaks in the carbon shells of the particles. F-SiO_2 particles do not have these two characteristic peaks, indicating that they are pure silica.

The carbon shell in the A-E series SiO_2@C particles was further characterized by Raman spectroscopy. In Fig. 6, the peaks at 1360 cm^{-1} and 1580 cm^{-1} correspond to the D band and G band of carbon, respectively. Additionally, the D and G peaks are broad. Combined with the electron microscope results, it can be seen that the shell is an amorphous carbon layer. The results of FTIR and Raman are consistent with the EDS spectrum, demonstrating that the RSSC particles are a porous carbon-coated silica material.

3.6. CMP performances

The polishing performance of abrasives is usually reflected by the material removal rate and the average surface roughness of the zirconia ceramic before and after polishing. According to Formula (1), the MRR (nm/h) of different abrasives is calculated by the mass difference Δm (g) of the zirconia ceramic before and after polishing.

$$MRR = \frac{\Delta m * 10^7}{\rho S T} \quad (1)$$

here, ρ is the density of the zirconia ceramic($g \cdot cm^{-3}$, $\rho_{zirconia} = 6.10\ g \cdot cm^{-3}$), S is the area of the zirconia ceramic (cm^2, 5.5 cm*5.5 cm), and *T* is the polishing time (h).

The MRR of spherical silica, A-SiO_2@C and F-SiO_2 abrasives is shown in Fig. 7(a). Under the same conditions, the removal rates of A-SiO_2@C abrasives (196.5 nm/h) and F-SiO_2 abrasives (243.8 nm/h) are both greater than that of spherical silica abrasives (142.3 nm/h), which shows that rod-shaped silica abrasives are more effective than spherical silica abrasives. This may be attributed to the special morphology of the rod-shaped abrasives which brings higher mechanical effect. Fig. 7 (b) shows the effect of different carbon coating contents in RSSC abrasives on MRR. The MRR values of the RSSC abrasives are all lower than that of the pure rod-shaped silica abrasives when the carbon coating content is less than 5.8 wt%. This may be due to the hardness of the carbon shell is lower [35], which reduces the overall hardness of the abrasives, which in turn makes their MRR lower than pure rod-shaped silica abrasives. Interestingly, as the carbon coating content increases, the curve of the MRR value of the RSSC abrasives first rises sharply and then gradually becomes flat. The continuous increase in MRR should be attributed to the difference in the structure of abrasives. In general, RSSC abrasives are better than SS abrasives in MRR. Especially when the carbon content of the coating reaches 5.8 wt%, the MRR of the

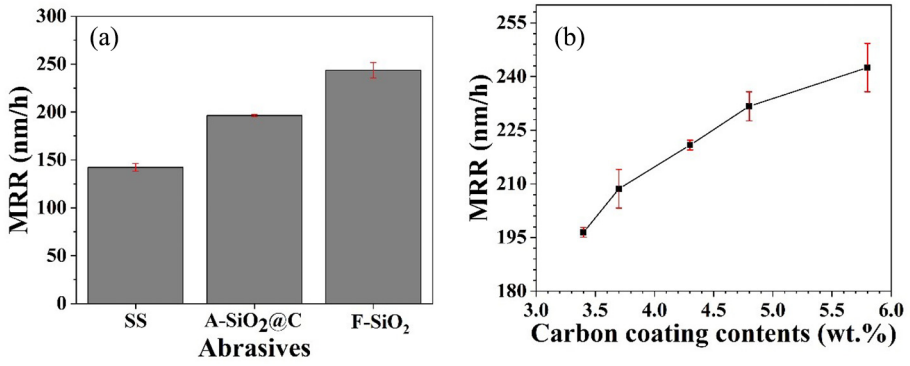

Fig. 7. (a) The MRR of SS, A-SiO_2@C and F-SiO_2. (b) The MRR of different RSSC abrasives (The red line is the error bar, and measured values are repeated 3 times).

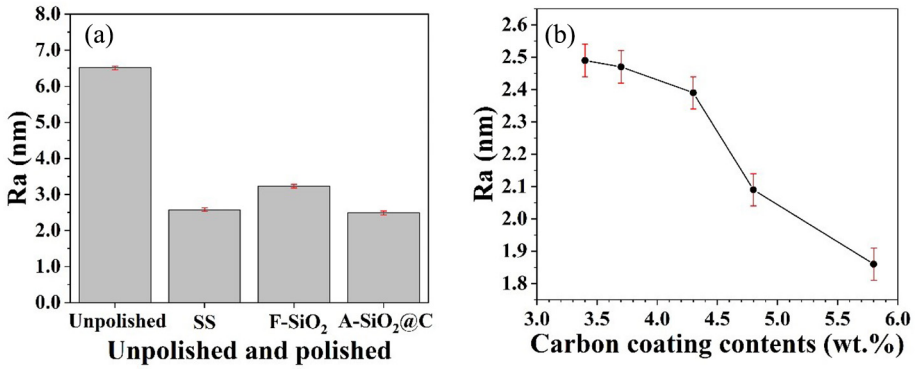

Fig. 8. (a) The Ra of zirconia ceramics before and after polishing with SS, F-SiO_2 and A -SiO_2@C slurries. (b) The Ra of zirconia ceramics after polishing with different RSSC abrasives (The red line is the error bar, and measured values are repeated 3 times).

RSSC abrasives reaches the highest value of 242.5 nm/h, which is increased by up to 70.4% (compared to the MRR of SS abrasives) and similar to the MRR of F-SiO_2 abrasives.

Ra is used to examine the polishing quality, that is, the planarization degree of zirconia ceramics. Fig. 8(a) shows the Ra of zirconia ceramics before and after polishing with three slurries. The original Ra of zirconia ceramic is 6.51 nm and Ra values are all reduced after polishing. Clearly, carbon-coated rod-shaped silica abrasives can achieve a lower surface roughness of 2.49 nm. This indicates that the rod-shaped carbon-coated silica abrasives can achieve a higher material removal rate

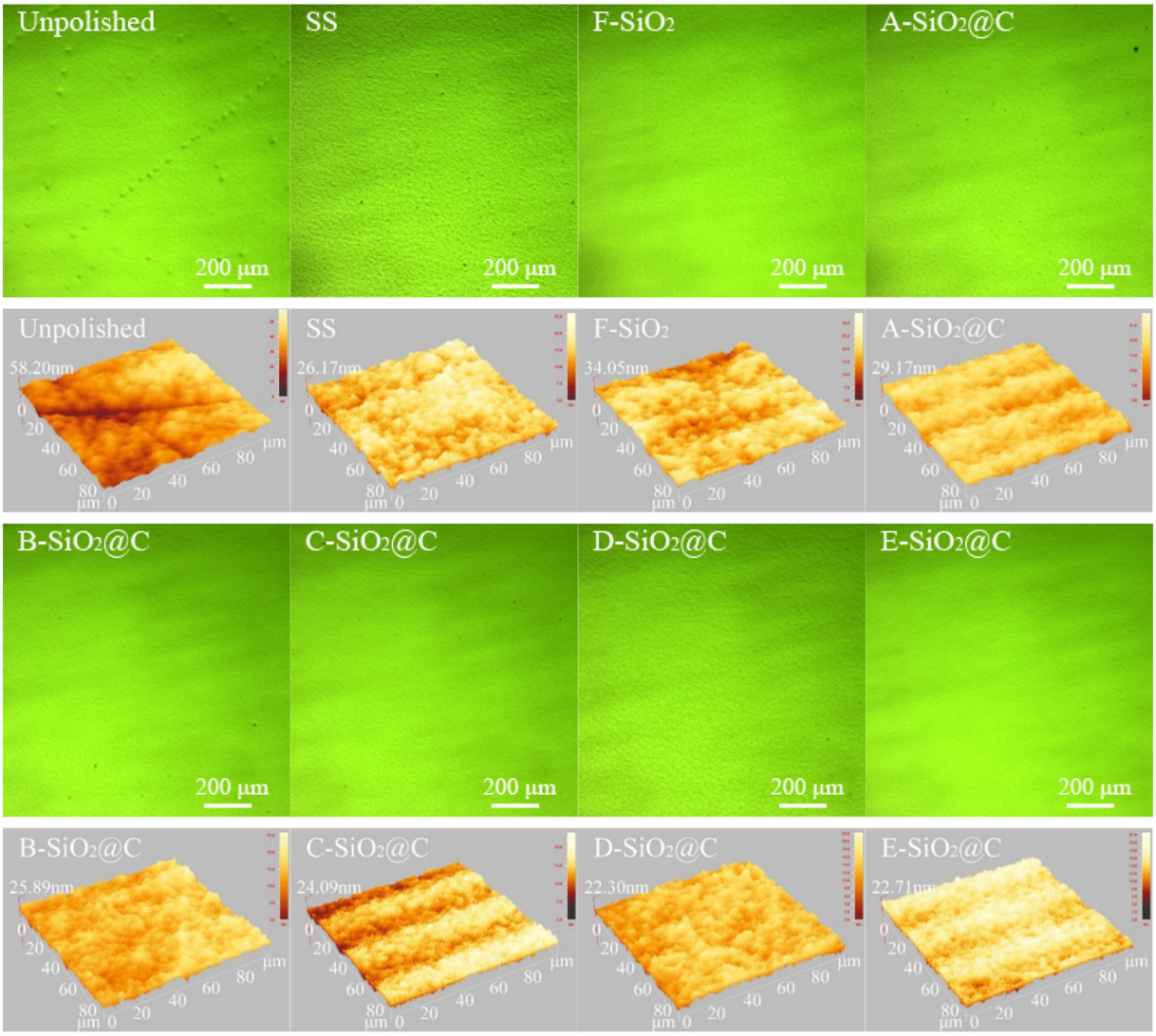

Fig. 9. Micrographs and corresponding three-dimensional images of the surface of zirconia ceramics before and after polishing with different abrasives.

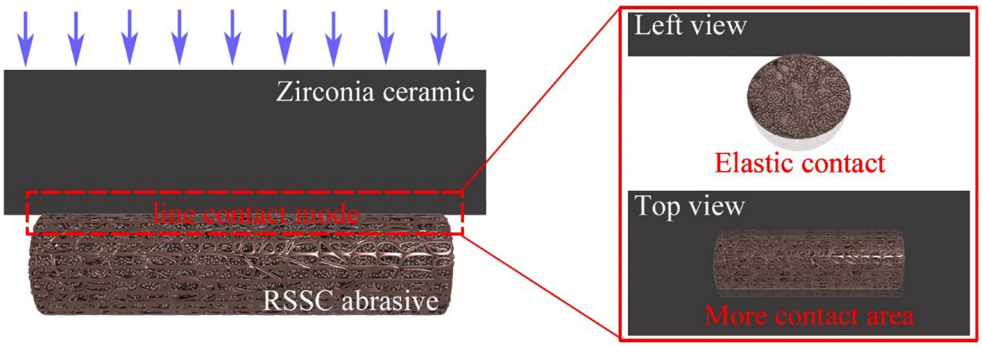

Fig. 10. Contact wear model of RSSC abrasives and zirconia ceramic.

while ensuring a lower surface roughness, showing better potential for industrial applications. The Ra values of zirconia ceramics polished by RSSC abrasives with different carbon coating contents are shown in Fig. 8(b). The surface roughness of zirconia ceramics gradually decreases with an increase in carbon coating content, reaching a minimum of 1.86 nm. This may be due to the core-shell structure of the carbon-coated silica abrasives. RSSC abrasives tend to be in elastic contact because of the lower hardness of carbon shell when they are in contact with the zirconia ceramic. This contact method can gradually reduce the scratches on the surface of the zirconia ceramic and prevent particles from causing secondary damage to the ceramic, thereby reducing the surface roughness of the zirconia ceramic [36].

Fig. 9 shows metallographic microscope images of zirconia ceramics before and after polishing with different abrasives and the corresponding three-dimensional (3D) topography measured by the surface profiler, providing more direct information. Among them, the low-frequency morphology observed in the 3D image is caused by the interference fringe of light, which does not affect the measurement of the sample surface. The surfaces of the zirconia ceramics before polishing had more scratches and large pores. Scratches and holes on the surfaces of the ceramics gradually disappeared, and the surface quality improved significantly after polishing. Spherical silica abrasives can reduce the overall roughness of the ceramic sheet, but the lowest surface roughness cannot be achieved in the same timeframe due to the low removal rate. Although pure rod-shaped silica abrasives can quickly achieve lower roughness, the figure shows that there are still shallow scratches on the ceramic surface. This is because pure rod-shaped silica abrasives may cause secondary damage on the ceramic surface, which will affect the surface quality. In addition, Fig. 9 shows that the scratches on the surface of the zirconia ceramic disappear as the carbon coating increases, and the large pores gradually shrink until they disappear. This is consistent with the Ra values measured using the surface profiler.

3.7. CMP mechanism of RSSC

It is well known that the CMP process involves both mechanical and chemical effects. The mechanical wear in the CMP process is mainly the friction and wear between the abrasives and the workpiece [37]. Therefore, the actual contact mode between abrasives and the workpiece plays a very important role in the polishing process. A contact wear model between rod-shaped carbon-coated silica abrasives and zirconia ceramics was established, as shown in Fig. 10. Due to the different morphology of RSSC and SS abrasives, the contact method between abrasives and zirconia is also completely different. Therefore, the effect of the tribochemical reaction will be different. Combined with the simple motion state animation of spherical and rod-shaped abrasives in the polishing process simulated by ADAMS (Fig. S4), it is not difficult to show that the contact between spherical abrasives and the wafer under pressure is a classic single-point contact. The contact mode between rod-shaped abrasives and the workpiece under pressure changes into line contact mode. Of course, in the actual polishing process, the contact between abrasives and the workpiece is often more complicated.

Table 2 shows the coefficient of friction (μ_s: coefficient of static friction, μ_k: dynamic friction factor) of all samples. As shown, the coefficient of friction of pure rod-shaped silica abrasives reaches a maximum ($\mu_s = 0.513$, $\mu_k = 0.417$). The μ_k of the A-E series abrasives is maintained at about 0.35, which is slightly lower than that of pure rod-shaped silica abrasives. This is mainly due to the carbon layer (carbon materials have a lubricating effect). However, all rod-shaped abrasives have higher coefficients of friction than spherical silica abrasives. Therefore, the RSSC abrasives have a stronger mechanical effect due to a higher coefficient of friction. This is why the MRR of rod-shaped abrasives is higher than that of SS abrasives.

The friction force in CMP wear is the sum of the resistance produced by the plough effect and the adhesion effect [38].

$$F = F_{ploughing} + F_{adhesion} \quad (2)$$

Line contact mode will also lead to an increase in the contact area between abrasives and zirconia ceramics, and the increase in contact area is conducive to increasing adhesion [24]. Abrasives may undergo elastic deformation in contact with the workpiece under a given load [39]. Fig. S5 shows the TEM image of the RSSC abrasive after polishing, and its morphology and structure are the same as before polishing. It shows that abrasives can indeed be elastically deformed. The elastic properties of *E*-SiO_2@C abrasives and pure SiO_2 abrasives were studied by AFM nano-indentation technology. Fig. 11 shows the typical force-z height curves of E-SiO_2@C abrasives and F-SiO_2 abrasives. The Young's modulus of E-SiO_2@C abrasives is 3.9 ± 0.7 GPa, and that of F-SiO_2 abrasives is 53.5 ± 1.2 GPa. It shows that RSSC abrasives do have higher elastic properties because of the carbon shell. Although the lower hardness of the carbon shell reduces the overall hardness of RSSC abrasives, resulting in the weakening of the plough effect. The higher elastic property makes the elastic deformation of RSSC abrasives larger, and the

Table 2
Coefficients of friction of different abrasives.

Abrasives	SS	A-SiO_2@C	B-SiO_2@C	C-SiO_2@C	D-SiO_2@C	E-SiO_2@C	F-SiO_2
μ_s	0.31	0.427	0.461	0.47	0.471	0.453	00.513
μ_k	0.265	0.355	0.353	0.351	0.358	0.347	00.417

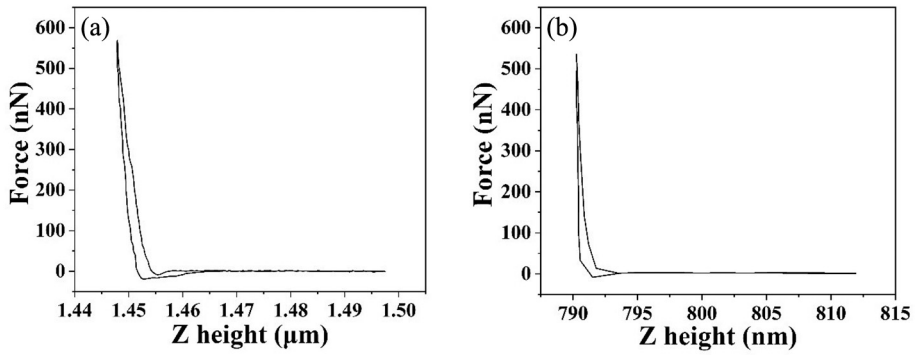

Fig. 11. Force-z height curves recorded on (a) E-SiO_2@C abrasives and (b) F-SiO_2 abrasives.

contact area between abrasives and the workpiece is larger, so the adhesion force is also greater. Mo et al. [40] pointed out that when elastic deformation occurs, the adhesion force will dominate the friction force. As the carbon content increases, the elastic properties will continue to increase. Although the plough force is gradually weakening, the dominant adhesion force will continue to increase. In addition, due to the continuous increase of the contact area, the load can be better distributed, so that the indentation becomes shallow and secondary damage can be reduced to obtain a better surface quality.

The chemical effect in CMP mainly includes the direct chemical corrosion of the workpiece by chemical reagents in the slurry [41] and the tribochemical effect between the abrasives and the workpiece [30]. Pores of some porous abrasives may adsorb the active chemical components in the slurry and increase the chemical reaction between the chemical components in the abrasives and the workpiece when they contact [39]. The hydroxylation of zirconia occurs on the surface in a moist environment, forming a surface reaction layer of -Zr-OH [42]. Then the surface reaction layer (Zr-OH) of zirconia is more easily removed under the mechanical action of abrasives. Qi et al. [43] reported that micro-porous silica can adsorb water molecules through pores, thereby promoting tribochemical reactions. In our experiment, the mesoporous carbon shell of RSSC abrasives can also absorb a certain amount of water molecules. The water molecules in the pores can continue to react with the zirconia surface when the abrasive contacts the workpiece, forming a dynamic tribochemical reaction. RSSC abrasives with higher and higher specific surface areas (as shown in Table 1) can adsorb more water molecules in the pores. Furthermore, when the abrasives come into elastic contact with the zirconia ceramic, the increase in the water molecules and the contact area can promote the tribochemical reaction between the two, thereby increasing the removal rate. This point can be further clarified based on the contact angle results for each slurry (Fig. 12). As the carbon coating content increases, the contact angle of the sample continues to decrease, and the particles tend to be more hydrophilic. The improvement of the hydrophilic nature of the slurry can contribute to increasing processing rates [44]. This also explains why MRR increases with the increasing carbon content.

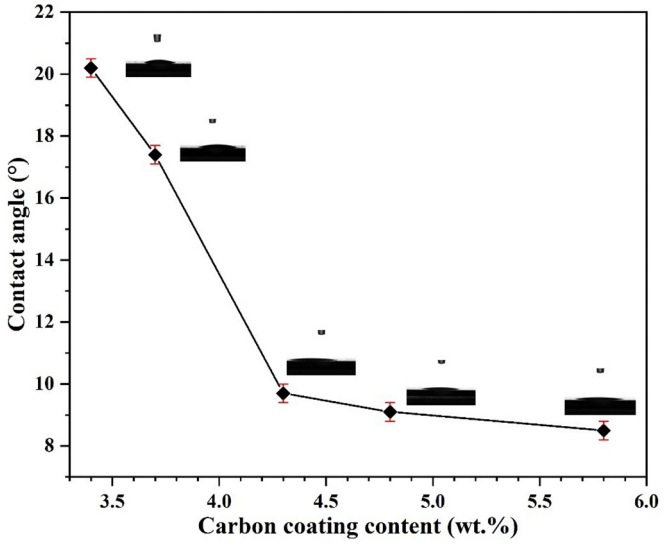

Fig. 12. Contact angles of abrasives with different carbon coating contents (The red line is the error bar, and measured values are repeated 3 times).

In conclusion, the removal mechanism of the RSSC abrasive is closely related to its rod-shaped morphology, core-shell structure and mesoporous structure. The surface planarization of the zirconia ceramic is achieved by the unique contact mode of RSSC abrasives, combined with adhesion and tribochemical effects during CMP.

4. Conclusions

In this study, rod-shaped silica seed crystals were prepared by the microemulsion template method, and then silicic acid was used to grow unevenly on the seed crystals. Finally, the rod-shaped SiO_2@C composite abrasives were formed by freeze-drying and calcination. The excellent polishing performance of rod-shaped SiO_2@C abrasives (MRR = 235.76 nm/h, Ra = 1.86 nm) is due to the morphologies and structures of particles. When rod-shaped SiO_2@C abrasives are in contact with zirconia ceramics, line contact mode can ensure a larger friction and effective contact area between particles and the workpiece. Furthermore, the overall hardness of abrasives is reduced and the elastic contact of abrasives is increased due to the core-shell structure, thereby improving the adhesion force and the ceramic surface quality. Rod-shaped SiO_2@C abrasives with a maximum specific surface area of 151.63 m^2/g can adsorb more water molecules and promote the tribochemical reaction. Rod-shaped SiO_2@C abrasives are promising non-spherical composite silica particles that can replace conventional spherical silica abrasives.

Declaration of Competing Interest

The authors declare that they have no known competing financial interests or personal relationships that could have appeared to influence the work reported in this paper.

Acknowledgements

This work was supported by the National Natural Science Foundation of China (Grant Number 51975343), Shanghai Technical Service Center for Advanced Ceramics Structure Design and Precision Manufacturing (No. 20DZ2294000) and the China Scholarship Council.

Appendix A. Supplementary data

Supplementary data to this article can be found online at https://doi.org/10.1016/j.powtec.2021.09.070.

References

[1] R.C. Garvie, R.H. Hannink, R.T. Pascoe, Ceramic steel? Nature. 258 (1975) 703–704, https://doi.org/10.1038/258703a0.

[2] Y. Chen, B. Fan, B. Yang, W. Ma, G. Liu, H. Li, Microwave sintering and fracture behavior of zirconia ceramics, Ceram. Int. 45 (2019) 17675–17680, https://doi.org/10.1016/j.ceramint.2019.05.334.

[3] R.H.J. Hannink, P.M. Kelly, B.C. Muddle, Transformation toughening in zirconia-containing ceramics, J. Am. Ceram. Soc. 83 (2000) 461–487, https://doi.org/10.1111/j.1151-2916.2000.tb01221.x.

[4] M. Behtash, J. Wong, S. Jiang, J. Luo, K. Yang, First-principles study of impurity segregation in zirconia, hafnia, and yttria-stabilized-zirconia grain boundaries, J. Eur. Ceram. Soc. 39 (2019) 3812–3820, https://doi.org/10.1016/j.jeurceramsoc.2019.04.039.

[5] T. Kumagai, Isostatic compaction behavior of yttria-stabilized tetragonal zirconia polycrystal powder granules, Powder Technol. 329 (2018) 345–352, https://doi.org/10.1016/j.powtec.2018.01.088.

[6] C. Li, Y. Wu, X. Li, L. Ma, F. Zhang, H. Huang, Deformation characteristics and surface generation modelling of crack-free grinding of GGG single crystals, J. Mater. Process. Technol. 279 (2020) 116577, https://doi.org/10.1016/j.jmatprotec.2019.116577.

[7] Y. Zhang, Q. Wang, C. Li, Y. Piao, N. Hou, K. Hu, Characterization of surface and subsurface defects induced by abrasive machining of optical crystals using grazing incidence X-ray diffraction and molecular dynamics, J. Adv. Res. (2021) https://doi.org/10.1016/j.jare.2021.05.006.

[8] C. Li, X. Li, S. Huang, L. Li, F. Zhang, Ultra-precision grinding of Gd3Ga5O12 crystals with graphene oxide coolant: material deformation mechanism and performance evaluation, J. Manuf. Process. 61 (2021) 417–427, https://doi.org/10.1016/j.jmapro.2020.11.037.

[9] X. Shi, L. Xu, Y. Zhou, C. Zou, R. Wang, G. Pan, An: in situ study of chemical-mechanical polishing behaviours on sapphire (0001) via simulating the chemical product-removal process by AFM-tapping mode in both liquid and air environments, Nanoscale. 10 (2018) 19692–19700, https://doi.org/10.1039/c8nr04645j.

[10] J. Wang, Y. Li, J. Han, Q. Xu, Y. Guo, Evaluating subsurface damage in optical glasses, J. Eur. Opt. Soc. 6 (2011) 11001, https://doi.org/10.2971/jeos.2011.11001.

[11] D. Yin, X. Niu, K. Zhang, J. Wang, Y. Cui, Preparation of MgO doped colloidal SiO2 abrasive and their chemical mechanical polishing performance on c-, r- and a-plane sapphire substrate, Ceram. Int. (2018) https://doi.org/10.1016/j.ceramint.2018.05.087.

[12] W. Xie, Z. Zhang, L. Liao, J. Liu, H. Su, S. Wang, D. Guo, Green chemical mechanical polishing of sapphire wafers using a novel slurry, Nanoscale. 12 (2020) 22518–22526, https://doi.org/10.1039/d0nr04705h.

[13] M.M. Rashad, M.M. Hessien, E.A. Abdel-Aal, K. El-Barawy, R.K. Singh, Transformation of silica fume into chemical mechanical polishing (CMP) nano-slurries for advanced semiconductor manufacturing, Powder Technol. 205 (2011) 149–154, https://doi.org/10.1016/j.powtec.2010.09.005.

[14] H. Aida, H. Takeda, T. Doi, Analysis of mechanically induced subsurface damage and its removal by chemical mechanical polishing for gallium nitride substrate, Precis. Eng. 67 (2021) 350–358, https://doi.org/10.1016/j.precisioneng.2020.10.007.

[15] Z. Zhang, L. Liao, X. Wang, W. Xie, D. Guo, Development of a novel chemical mechanical polishing slurry and its polishing mechanisms on a nickel alloy, Appl. Surf. Sci. 506 (2020) 144670, https://doi.org/10.1016/j.apsusc.2019.144670.

[16] M.H. Oh, J.S. Nho, S.B. Cho, J.S. Lee, R.K. Singh, Polishing behaviors of ceria abrasives on silicon dioxide and silicon nitride CMP, Powder Technol. 206 (2011) 239–245, https://doi.org/10.1016/j.powtec.2010.09.025.

[17] P.B. Zantye, A. Kumar, A.K. Sikder, Chemical Mechanical Planarization for Microelectronics Applications, 2004 https://doi.org/10.1016/j.mser.2004.06.002.

[18] J. Li, Y. Zhu, C. Chen, Chemical mechanical polishing of transparent Nd:YAG ceramics, Key Eng. Mater. 375–376 (2008) 278–282, https://doi.org/10.4028/www.scientific.net/kem.375-376.278.

[19] G. Liu, Z. Huang, X. Liu, D. Jiang, Removal behaviors of different SiC ceramics during polishing, J. Mater. Sci. Technol. 26 (2010) 125–130, https://doi.org/10.1016/S1005-0302(10)60020-5.

[20] X. Shi, G. Pan, Y. Zhou, Z. Gu, H. Gong, C. Zou, Characterization of colloidal silica abrasives with different sizes and their chemical-mechanical polishing performance on 4H-SiC (0001), Appl. Surf. Sci. 307 (2014) 414–427, https://doi.org/10.1016/j.apsusc.2014.04.048.

[21] C. Liang, L. Wang, W. Liu, Z. Song, Non-spherical colloidal silica particles-preparation, application and model, Colloids Surfaces A Physicochem. Eng. Asp. 457 (2014) 67–72, https://doi.org/10.1016/j.colsurfa.2014.05.053.

[22] S. Salleh, I. Sudin, A. Awang, Effects of non-spherical colloidal silica slurry on Al-NiP hard disk substrate CMP application, Appl. Surf. Sci. 360 (2016) 59–68, https://doi.org/10.1016/j.apsusc.2015.10.169.

[23] L. Xu, H. Lei, T. Wang, Y. Dong, S. Dai, Preparation of flower-shaped silica abrasives by double system template method and its effect on polishing performance of sapphire wafers, Ceram. Int. 45 (2019) 8471–8476, https://doi.org/10.1016/j.ceramint.2019.01.158.

[24] S. Dai, H. Lei, J. Fu, Self-assembly preparation of popcorn-like colloidal silica and its application on chemical mechanical polishing of zirconia ceramic, Ceram. Int. 46 (2020) 24225–24230, https://doi.org/10.1016/j.ceramint.2020.06.202.

[25] J.-D. Lee, Y.-R. Park, B.U. Yoon, Y.-P. Han, S. Hah, J.-T. Moon, Effects of nonionic surfactants on oxide-to-polysilicon selectivity during chemical mechanical polishing, J. Electrochem. Soc. 149 (2002) G477, https://doi.org/10.1149/1.1488650.

[26] S. Armini, J. De Messemaeker, C.M. Whelan, M. Moinpour, K. Maex, Composite polymer core–ceria shell abrasive particles during oxide CMP: a defectivity study, J. Electrochem. Soc. 155 (2008) 653–660, https://doi.org/10.1149/1.2949085.

[27] Y. Chen, W. Mu, J. Lu, Young's modulus of PS/CeO 2 composite with core/shell structure microspheres measured using atomic force microscopy, J. Nanopart. Res. 14 (2012) 696, https://doi.org/10.1007/s11051-011-0696-1.

[28] Y. Chen, Z. Mu, W. Wang, A. Chen, Development of mesoporous SiO2/CeO2 core/shell nanoparticles with tunable structures for non-damage and efficient polishing, Ceram. Int. 46 (2020) 4670–4678, https://doi.org/10.1016/j.ceramint.2019.10.198.

[29] N. Bun-Athuek, H. Takazaki, Y. Yoshimoto, P. Khajornrungruang, T. Yasunaga, K. Suzuki, Effects of mixed ultrafine colloidal silica particles on chemical mechanical polishing of sapphire, Jpn. J. Appl. Phys. 57 (2018), 07MD03 https://doi.org/10.7567/JJAP.57.07MD03.

[30] L. Xu, H. Lei, Nano-scale surface of ZrO2 ceramics achieved efficiently by peanut-shaped and heart-shaped SiO2 abrasives through chemical mechanical polishing, Ceram. Int. 46 (2020) 13297–13306.

[31] A. Kuijk, A. Van Blaaderen, A. Imhof, Synthesis of monodisperse, rodlike silica colloids with tunable aspect ratio, J. Am. Chem. Soc. 133 (2011) 2346–2349, https://doi.org/10.1021/ja109524h.

[32] R.P. Murphy, K. Hong, N.J. Wagner, Synthetic control of the size, shape, and polydispersity of anisotropic silica colloids, J. Colloid Interface Sci. 501 (2017) 45–53, https://doi.org/10.1016/j.jcis.2017.04.026.

[33] A. Lazaro, M.C. Van De Griend, H.J.H. Brouwers, J.W. Geus, The influence of process conditions and Ostwald ripening on the specific surface area of olivine nano-silica, Microporous Mesoporous Mater. 181 (2013) 254–261, https://doi.org/10.1016/j.micromeso.2013.08.006.

[34] P. Kokhanenko, K. Brown, M. Jermy, Silica aquasols of incipient instability: synthesis, growth kinetics and long term stability, Colloids Surfaces A Physicochem. Eng. Asp. 493 (2016) 18–31, https://doi.org/10.1016/j.colsurfa.2015.10.026.

[35] J. Robertson, Amorphous carbon, Adv. Phys. 60 (2011) 87–144, https://doi.org/10.1080/00018732.2011.534871.

[36] W.C. Oliver, F.R. Brotzen, On the generality of the relationship among contact stiffness, contact area, and elastic modulus during indentation, J. Mater. Res. 7 (1992) 613–617, https://doi.org/10.1557/JMR.1992.0613.

[37] J. Luo, D.A. Dornfeld, Material removal mechanism in chemical mechanical polishing: theory and modeling, IEEE Trans. Semicond. Manuf. 14 (2001) 112–133, https://doi.org/10.1109/66.920723.

[38] P.Z. Zhu, Y.Z. Hu, T.B. Ma, H. Wang, Molecular dynamics study on friction due to ploughing and adhesion in nanometric scratching process, Tribol. Lett. 41 (2011) 41–46, https://doi.org/10.1007/s11249-010-9681-6.

[39] A. Chen, Y. Chen, X. Zhao, Y. Wang, Core/shell structured PS/mSiO2 hybrid particles: controlled preparation, mechanical property, and their size-dependent CMP performance, J. Alloys Compd. 779 (2019) 511–520, https://doi.org/10.1016/j.jallcom.2018.11.314.

[40] Y. Mo, K.T. Turner, I. Szlufarska, Friction laws at the nanoscale, Nature. 457 (2009) 1116–1119, https://doi.org/10.1038/nature07748.

[41] C. Huang, W. Mu, H. Zhou, Y. Zhu, X. Xu, Z. Jia, L. Zheng, X. Tao, Effect of OH- on chemical mechanical polishing of β-Ga2O3 (100) substrate using an alkaline slurry, RSC Adv. 8 (2018) 6544–6550, https://doi.org/10.1039/c7ra11570a.

[42] U. Lohbauer, M. Zipperle, K. Rischka, A. Petschelt, F.A. Müller, Hydroxylation of dental zirconia surfaces: characterization and bonding potential, J. Biomed. Mater. Res. - Part B Appl. Biomater. 87 (2008) 461–467, https://doi.org/10.1002/jbm.b.31126.

[43] Y. Qi, L. Chen, S. Jiang, J. Yu, B. Yu, C. Xiao, L. Qian, Investigation of silicon wear against non-porous and micro-porous SiO2 spheres in water and in humid air, RSC Adv. 6 (2016) 89627–89634, https://doi.org/10.1039/c6ra18152j.

[44] P.S.K. Toshiro Doi, Ioan D. Marinescu, Advances in CMP/Polishing Technologies For The Manufacture Of Electronic Devices, 2012 https://doi.org/10.1016/B978-1-4377-7859-5.X0001-4.